Tribology International 179 (2023) 108206

Contents lists available at ScienceDirect

Tribology International

journal homepage: www.elsevier.com/locate/triboint

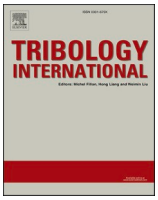

Tribological behavior of molybdenum disulfide and tungsten disulfide sprayed coatings in low viscosity hydrocarbon environments

E. Cairns [a], A. Ayyagari [a], C. McCoy [a], S. Berkebile [b], D. Berman [a,*], S.M. Aouadi [a,*], A.A. Voevodin [a,*]

[a] Department of Materials Science and Engineering, University of North Texas, Denton TX 76203, USA
[b] US DEVCOM Army Research Laboratory, Aberdeen Proving Ground, MD 21005, USA

ARTICLE INFO

Keywords:
Transition metal dichalcogenides
Sprayed coatings
Sliding wear
Low viscosity hydrocarbons

ABSTRACT

The tribological behavior of MoS_2 and WS_2 transition metal dichalcogenide (TMD) spray coatings in low-viscosity hydrocarbon environments was investigated. Sliding tests were performed in two hydrocarbons – hydrophilic ethanol and hydrophobic dodecane and were compared to tests in humid air and dry nitrogen conditions. Coating steel surfaces decreased friction across all test conditions, with the largest and most sustainable decreases being in dry nitrogen and dodecane environments, where friction coefficients of less than 0.1 were sustained. Analysis was performed using scanning electron microscopy, Raman spectroscopy, and x-ray photoelectron spectroscopy. Friction reductions in dodecane were explained by reduced oxidation of the coating, due to protection from the hydrophobic hydrocarbon film, allowing basal plane alignment and uninhibited sliding of TMD sheets.

1. Introduction

The significance of solid lubricants for the mitigation of wear and frictional losses is widely established [1–3]. The recently growing interest for the expansion of solid lubricant use is supported by emerging oil-free lubrication applications [4], such as wind turbines [5], dry seal valves, forging and extrusion in manufacturing [6], propulsion, and flight control components in commercial space access industry [7,8]. Expanding solid lubricant use is also addressing the societal need to become less dependent on crude-oil-derived lubrication [9] for the reduction of environmental impact from oil processing and disposal. Hexagonal-based solids with easy-to-shear basal-oriented planes represent a dominant class of solid lubricants [10] offering alternatives to oil lubrication [3,11]. Prominent examples are transition metal dichalcogenides (TMDs) MoS_2 [12–14] and WS_2 [15], which provide extremely low friction at sliding interfaces in low-humidity and vacuum environments [11,16] and under moderate temperature conditions [17]. For hexagonal TMDs, several well-established tribological mechanisms of operation in ambient and vacuum environments are established, which include: the reorientation of basal planes to be parallel to sliding surfaces as a result of repeated mechanical straining [18,19], the increased crystallinity of TMD film surfaces under these recurring stresses, the accelerated oxidation of TMDs in humid ambient conditions with water and oxygen attachments to the edge of basal planes and to point defects, such as S vacancies, in the planes leading to inhibiting of shear [12,20,21], as well as their transition to abrasive oxides in air at elevated temperatures [14,22]. TMD materials are also used as particulate additives in oils to enhance their performance and increase wear life [23].

The literature on the use of TMD-based coatings in synthetic oil lubricating contacts and at sliding surfaces in low viscosity hydrocarbon fuels is scarce. However, several available reports indicate a favorable synergistic behavior for such combination. For example, in a recent paper by Singh et al. [24], titanium-doped MoS_2 coatings tested in polyalphaolefin oil (PAO) had shown the formation of a graphitic film in the wear track formed in rolling contact tests due to the decomposition of PAO as a result of the catalytic effect of Mo and MoS_2. The tribological behavior of TMD solid lubricant coatings in low viscosity hydrocarbon fuels is yet largely unexplored all together. At the same time, the emerging applications with the use of ethanol, methanol, synthetic alkane, and other low carbon emission fuels in combustion engines lead to a growing need for such studies especially for improving the wear endurance of fuel pump components that currently fail due to scuffing [25]. Knowing the strong dependence of TMDs on the presence of moisture, this study compared MoS_2 and WS_2 solid lubricant coating

* Corresponding authors.
E-mail addresses: Diana.Berman@unt.edu (D. Berman), Samir.Aouadi@unt.edu (S.M. Aouadi), Andrey.Voevodin@unt.edu (A.A. Voevodin).

https://doi.org/10.1016/j.triboint.2022.108206
Received 25 October 2022; Received in revised form 12 December 2022; Accepted 27 December 2022
Available online 28 December 2022

behavior immersed in low viscosity hydrocarbons with a high and low affinity to water, namely ethanol and dodecane. The test conditions were set in both humid air and dry nitrogen and thus provide insight into the wear mechanisms of TMDs in sliding contact with hydrocarbons. Test results were correlated with surface morphological and analytical investigations of worn surfaces to extract the important governing mechanisms.

2. Experimental

2.1. Coating preparation

The steps of the coating preparation are shown in Fig. 1. MoS_2 and WS_2 coatings were prepared on AISI 52100 steel disk coupons with a hardness of 61 HRC by a spray method using industrial-grade nanocrystalline powders of MoS_2 and WS_2 purchased from Graphene Supermarket. These powders had a nearly spherical morphology with an average particle size of 90 nm. Three grams of the TMD powders were added to 15 mL of ethanol, sonicated for 15 min, and tumbled to retain the solid materials in a uniform suspension. The suspensions were then spray-coated onto the polished steel discs (R_a = 60 nm), which were preheated to 160 °C. The spray-coating process parameters (air-line flow rate, air-brush spray rate, and line pressure) were optimized such that a fine nano-droplet mist of ethanol-bearing lubricant particles was produced. The ethanol carrier evaporated immediately upon contacting the surface of the hot steel substrate, depositing the contained solids. Multiple passes were applied to attain a uniform coating across the sample surface. A total of 3 mL of the solution (0.6 g of the solid lubricant) was deposited onto each steel surface that resulted in a coating thickness of 10–15 μm and an average coating roughness R_a of 1–2 μm. Thickness steps were created by placing masking tape at the center of the steel discs prior to deposition. Coating roughness and thickness were measured using a Zygo ZeGage Plus 3D Optical Profiler System.

2.2. Tribological tests

Tribological testing was carried out in a pin-on-disk Anton Paar TRB3 tribometer in unlubricated humid ambient air, dry nitrogen, and lubricated ethanol and dodecane environments at room temperature. For tests in ethanol and dodecane environments, the samples were completely immersed in 10 mL of low viscosity hydrocarbon fluid and tested in the ambient air. The relative air humidity for the ambient environment tests was in the range of 40–50%. The relative humidity for dry nitrogen tests was found to be less than 0.1%. For all tests, the counterface was a hardened 52100 steel ball (61 HRC) of 12 mm diameter. The tests were carried out using a constant 0.1 m/s sliding velocity and a 5 N load, corresponding to a maximum initial Hertz contact pressure of 1.1 GPa. The total sliding distance was kept constant at 100 m.

2.3. Characterization after tests

The wear of the tribopairs was measured using a Zeiss LSM 700 Optical Microscope. Raman spectra of the pristine coating materials prior to the tests and from within the sliding wear path (tribolayer) were acquired using a Renishaw Raman microscope with a 457 nm wavelength blue laser. Wear scar morphologies, and elemental changes were recorded using a Hitachi SV3500 tabletop Scanning Electron Microscope (SEM) with a Back-Scatter Emission (BSE) detector and 15 kV accelerating voltage. The SEM was equipped with an Oxford Xplore Energy Dispersive Spectrometer (EDS) for elemental identification. X-ray Photoemission Spectroscopy (XPS) spectra were measured using a PHI 5000 Versaprobe Scanning XPS Microprobe with monochromatic 1486.6 eV Al Kα radiation to analyze chemical changes in the wear track after sliding. Survey XPS spectra were collected over the binding energy range of 0 – 1100 eV. High-resolution XPS spectra were collected with an energy step size of 0.1 eV for Mo 3d, S 2p, C 1s, and O 1s regions. A charge referencing was performed for all scants using adventitious carbon on the sample surfaces with C 1s peak central position assumed at 284.50 eV.

3. Results and Discussion

3.1. Morphology and tribological behavior in pin-on-disk tests

Fig. 2 shows the morphology for the as-deposited coating at high magnification, where MoS_2 is used as a representative case. The spray powder deposition process resulted in thick (10–15 μm) coatings. The as-deposited coatings had a roughness of 1–3 μm R_a. The morphology showed agglomerated nanocrystalline powders sitting loosely on the surface.

The addition of TMD coatings onto the steel resulted in a decrease in the average coefficient of friction (COF) in all environments compared to

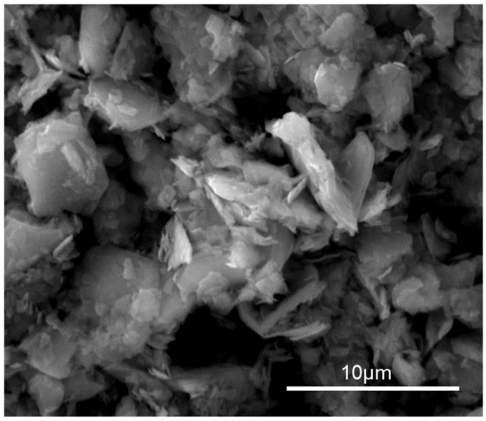

Fig. 2. BSE-SEM image of as-deposited MoS_2 coating surface.

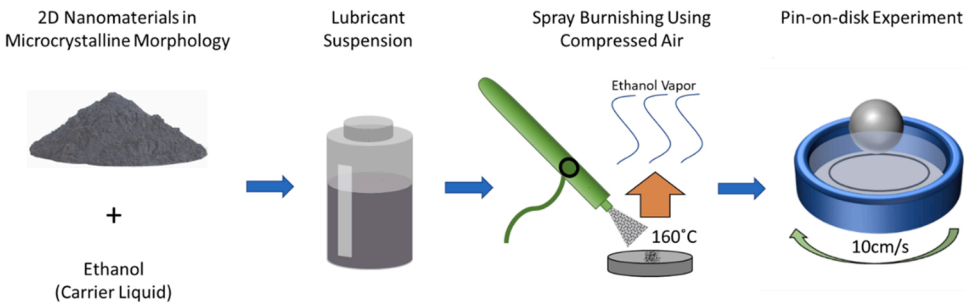

Fig. 1. Schematic of the experimental steps adopted in the tests.

the bare steel samples. Fig. 3 compares steady-state COFs for the tested coating and the bare substrates. For all coatings, the steady-state values were averaged over 50–100 m of sliding distance corresponding to after the running-in period when a steady-state COF was established. One deviation was tests in ethanol, where the steady-state COFs were averaged over 10–40 m sliding tests before the onset of failure of the coating as will be discussed later in the text. Large differences between coated and uncoated samples were seen in the dry nitrogen and humid air conditions, where direct steel-on-steel contact occurred for the uncoated samples leading to high friction. In the case of bare steel in humid air, the oxidative wear mechanisms resulted in an average friction value in the vicinity of 0.6. The use of TMD coatings resulted in the significant reduction in COF values over the bare steel. However, this reduction also depended on the test environment, where dry nitrogen and dodecane yielded the lowest steady-state measured COF values of coated samples. The reduction of COFs in dry nitrogen was well expected and attributed to a formation of lubricious tribolayers under sliding conditions as the TMD powders densified and reoriented with an easy-to-shear basal plane to be parallel to the sliding contact, following the mechanism which has been well documented in the literature [11,14]. Furthermore, previous studies confirmed that the ability to facilitate near-frictionless sliding in an oriented MoS_2 structure was highly dependent on the absence of water vapor near the sliding interface [18,26], which explains the difference in friction between dry nitrogen and humid air environments for MoS_2 coated samples. For the WS_2 coatings, this environmental difference in COFs was also measured. The difference was much less pronounced than for MoS_2, as WS_2 is known to be more resilient to oxidation and humid air [27].

The representative COF traces from the performed tests are shown in Fig. 4, from which it can be concluded that there was a quick decrease in friction in the coated samples during the running-in stages of the tests within the first one to five meters of sliding. For the MoS_2 and WS_2 coated samples tests in humid air (Fig. 4a), dry nitrogen (Fig. 4b), and dodecane (Fig. 4d), steady state COF values were achieved after an initial running-in period. This was attributed to the formation of the transfer films (optical images are presented in the next section) after the accumulation of sliding cycles needed for a reorientation of the grains of the TMD microstructure such that basal planes are aligned parallel to the sliding direction and provide stable and easy to shear molecular layers in the sliding contact. A decrease in friction occurred in the first few cycles in every condition other than humid air, where the competing processes of oxidation interfered and reduced the effectiveness of the TMD lubrication mechanism [3,11,14,28]. For tests in ethanol (Fig. 4c), the COF for both coatings displayed an initial running-in period, followed by a low friction period and then started rapidly climbing to COF levels comparable to those observed for uncoated substrates. This behavior was attributed to rapid wear through with the absence of the lubricating interfacial transfer film formation as confirmed by optical microscopy of counterbody surfaces presented next.

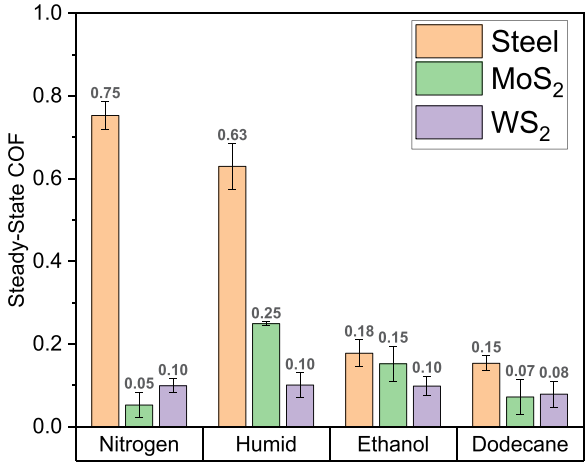

Fig. 3. Bar chart comparison of averaged steady-state COF values of MoS_2 coating, WS_2 coating, and uncoated 52100 steel in the investigated test environment conditions.

3.2. Optical microscopy analyses of sliding wear surfaces

Fig. 5 provides a summary of the optical analysis of the counterbody ball surfaces, yielding insights into the presence of the transfer solid lubricant films in the sliding contact areas.

The images in Fig. 5 show that both MoS_2 and WS_2 coatings resulted in transfer film formation on the steel counterface in the dry nitrogen conditions, which corresponds to the consistent and low friction values seen in Fig. 4(a). It was well expected that for dry sliding conditions, TMD coatings adhere and form a lubricious transfer layer on an uncoated counterface steel ball contact surface area. The MoS_2 and WS_2 and phase composition of such transfer films visible on the countre body was confirmed by the Raman analysis (see Supplemental) performed on the wear spots. Interestingly, the morphology of the transfer film was different for the two coatings. In the case of MoS_2, much more transfer film build-up in and around the area of contact could be seen, whereas in the case of WS_2 only a small amount of transfer film was observed immediately around the area of contact, which may be attributed to a difference in the adhesion of the MoS_2 and WS_2 transfer films to the counterpart steel ball. This is also supported by Raman analysis (see Supplemental) from inside the wear scars, which showed weak characteristic Raman spectra for WS_2. The presence of ethanol and dodecane clearly affected the ability of the coating to form a uniform transfer film on the steel counterfaces. For example, in dodecane-lubricated MoS_2, a thick transfer film can be seen in and around the wear scar, obscuring the steel ball wear spot. However, in the case of dodecane-lubricated WS_2, the wear spot is clearly visible and debris can be seen in the surrounding areas. For the counterfaces analysis after the tests in ethanol, no uniform transfer film was found, as well very little debris can be seen surrounding the wear scar. An absence of a uniform transfer film is also observed in humid air conditions, however, debris is seen around the wear spot without much residing within for both MoS_2 and WS_2.

3.3. Compositional analyses of wear tracks with SEM/EDS

SEM/EDS analysis was performed on wear tracks and the results are presented in Fig. 6 as elemental composition maps. Consistent with the optical imaging of the counterpart balls, EDS analysis of wear tracks revealed that there is a clear removal of TMD solid lubricant from the contact surface during sliding in ethanol, as evidenced by the lack of Mo Lα1 and W Mα1 fluorescence signal from inside the wear track. The removal of the coating in ethanol explains the rapid increase in friction during the test as presented in Fig. 4c. From the EDS results in Fig. 6, there also appears to be some removal of WS_2 from the wear track in the nitrogen and dodecane environments, despite the low friction recorded over the duration of these tests (see Figs. 4a and 4d). It is possible that during the run-in stage, some sprayed TMD powders were removed from the interface and pushed out of the contact area, while a thin layer of the reoriented coating remained in the center, facilitating the low friction performance seen in Fig. 4b and d. A very thin layer of the coating would show a Fe Kα1 signal from underneath due to an order of 1–2 μm penetration depth of the EDS analysis, and the contribution from the coating elements would be significantly diminished even as the low friction values may indicate the coating presence. For further characterization of the wear track phases and chemistry, more surface-sensitive Raman and XPS analyses were performed.

3.4. Wear track phase analysis with Raman spectroscopy

To provide insight into the dominant phases present in the wear

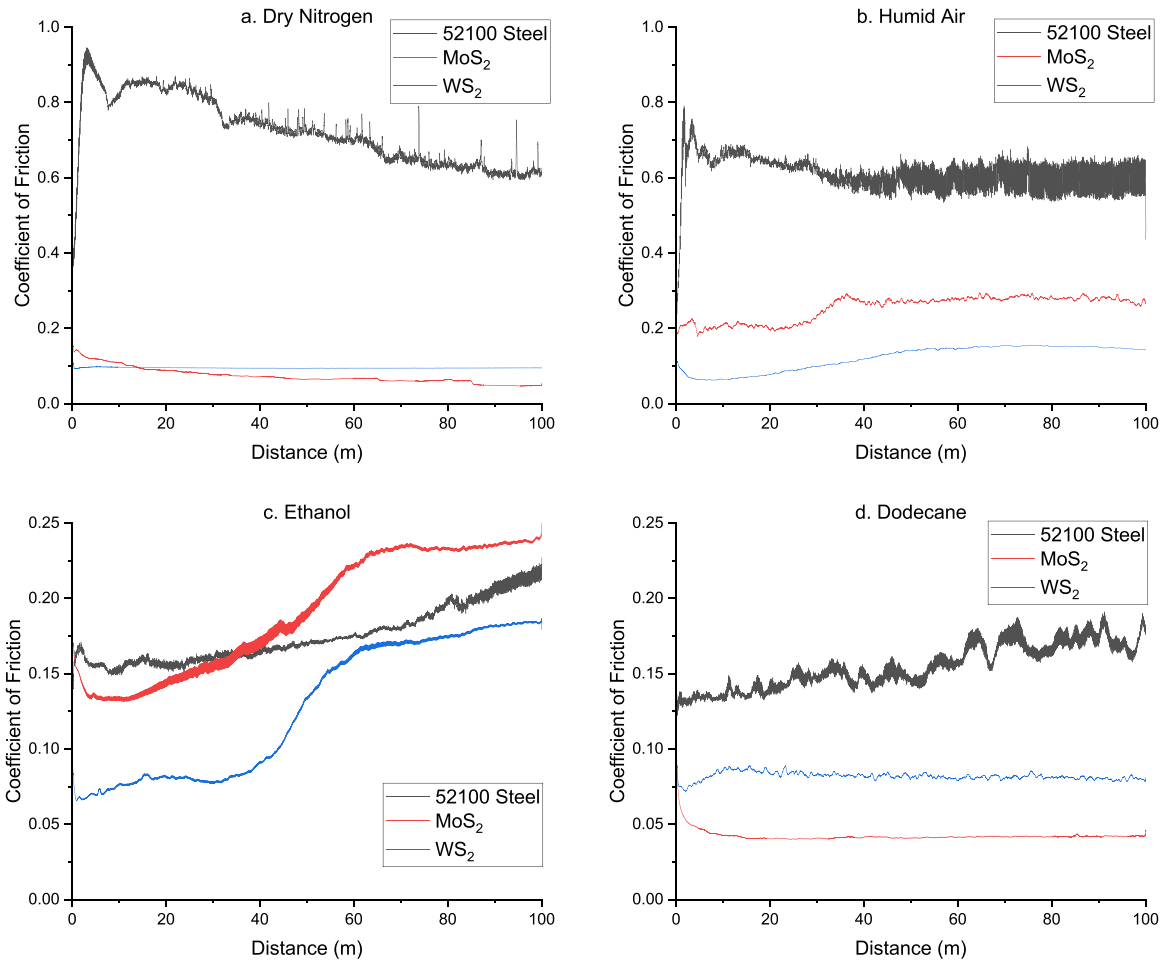

Fig. 4. COF plot comparisons of uncoated 52100 steel, MoS_2, and WS_2 coatings in a) dry nitrogen, b) humid air, c) ethanol, and d) dodecane environments.

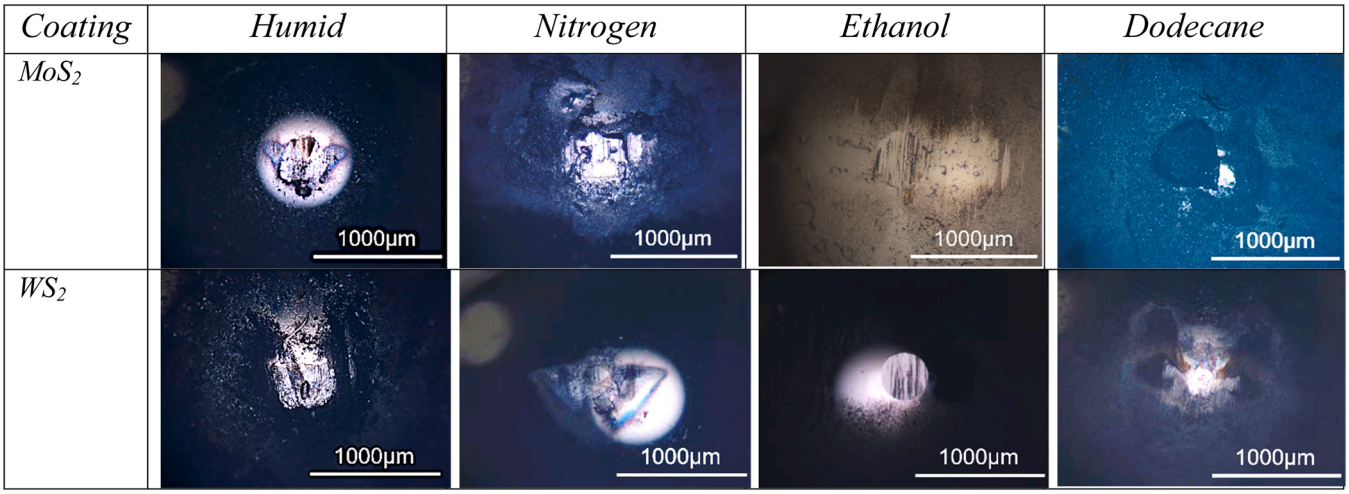

Fig. 5. Images of 52100 steel ball counterfaces after friction tests in humid, nitrogen, ethanol, and dodecane against MoS_2 and WS_2 coated samples.

tracks of the tested TMD coatings in low-viscosity hydrocarbon fuel environments, Raman spectroscopy was performed on samples after sliding by performing line scans across the wear track and tracking the evolution of the Raman spectra inside and outside the worn surfaces. Tests in ethanol, dodecane, and dry nitrogen were compared. Dry nitrogen served as a control baseline since Raman spectroscopic studies of TMDs have been performed previously and lubrication mechanisms are widely established [29–32]. Raman spectra analysis was performed using vibrational peaks characteristic for the 2H MoS_2 phase: E_{2g} and A_{1g}, which account for the in-plane and out-of-plane optical vibration modes, respectively, and are found at shifts of 383 and 408 cm^{-1}. Previous Raman studies of MoS_2 have been able to find correlations between peak spacing, peak width, and peak ratio with the layer thickness [32], grain size, and grain orientation [29], respectively. Similarly, the

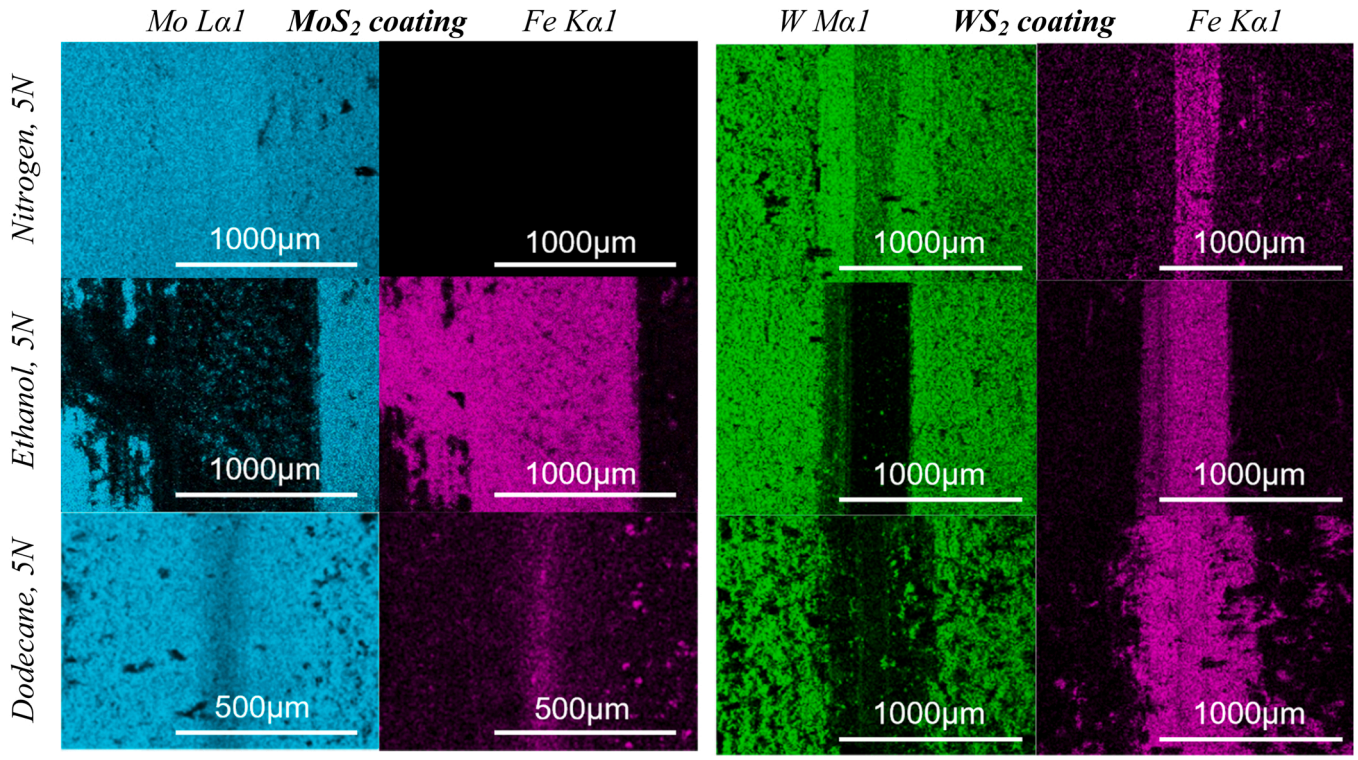

Fig. 6. SEM/EDS elemental maps of wear tracks on the surface of MoS_2 (left) and WS_2 (right) coatings after friction tests in dry nitrogen, ethanol, and dodecane in corresponding image rows.

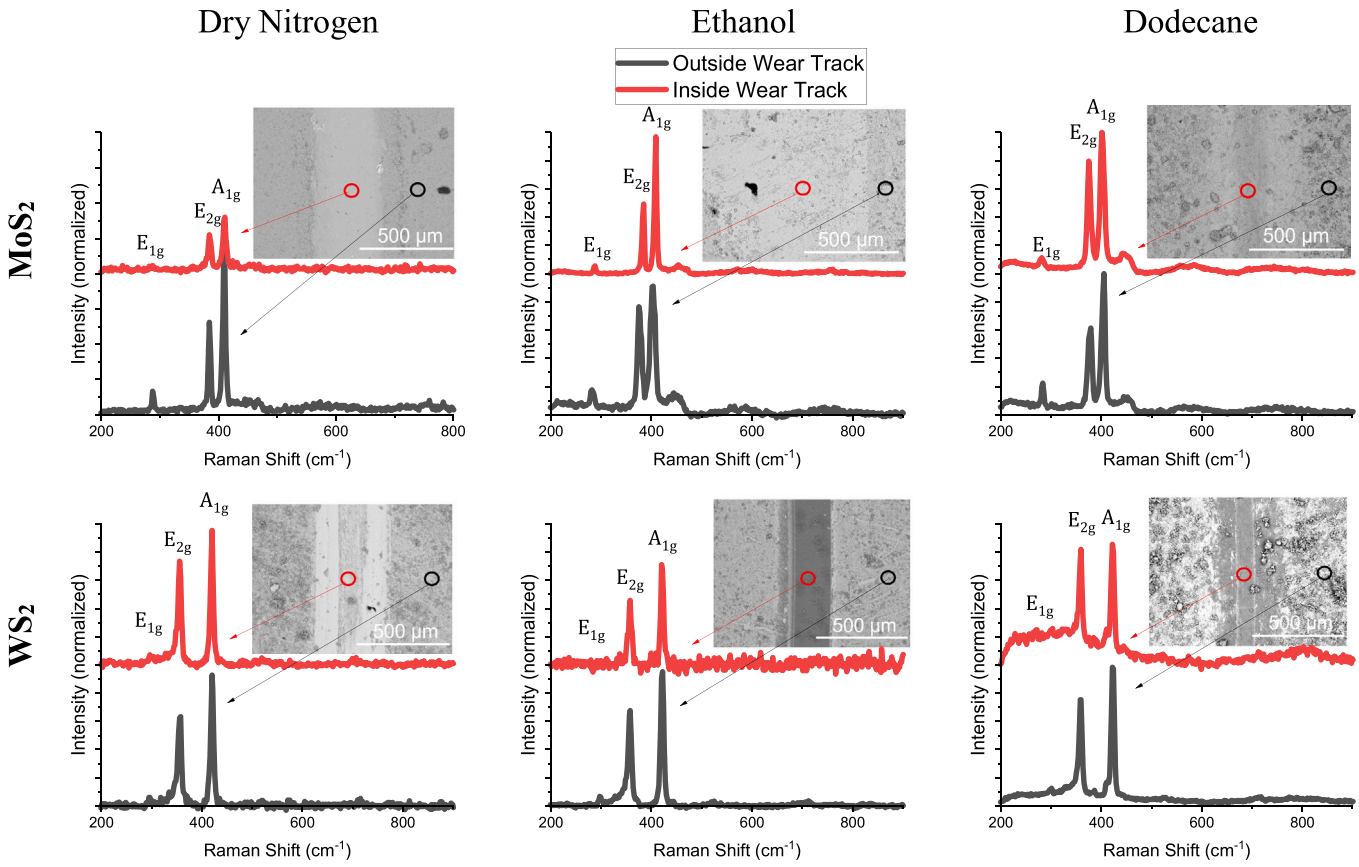

Fig. 7. Representative Raman analysis spectra collected from locations inside and outside wear tracks on the surface of MoS_2 coatings (top row) and WS_2 coatings (bottom row) after friction tests in dry nitrogen, ethanol, and dodecane in corresponding columns. Locations for spectra taken are indicated by black and red circles on SEM images overlayed above the spectra.

characteristic peaks of 353 and 418 cm^{-1} for the same E_{2g} and A_{1g}, vibrational modes of the 2H WS_2 phase were used for the analyses of wear tracks on WS_2 coated samples.

Representative Raman spectra, taken from points inside and outside the wear track (Fig. 7) revealed the presence of both hexagonal MoS_2 and WS_2 phases confirmed by primary Raman peaks of these phases. The presence of primary peaks both inside and outside the wear track in both the ethanol and dodecane conditions confirmed the comment made in the SEM/EDS result discussion section, that a thin TMD layer present inside the wear track may not be captured by EDS due to its limited surface sensitivity. Consistently with EDS results in Fig. 6, there was a notable decrease in signal-to-noise ratio inside the track in ethanol (see spectrum for WS_2 in Fig. 7) that indicates less material present. For WS_2 in ethanol, some regions in the center of the track did not display any Raman peak signals indicating the lack of TMD in such regions.

Table 1 shows calculated values for characteristic Raman E_{2g} and A_{1g} duplet peak spacing, full width at half maximum (FWHM), and their intensity ratios inside and outside the wear track for MoS_2 as a representative case. Both MoS_2 and WS_2 have shown similar COF evolutions and transfer film formation behaviors presented in the previous sections, and detailed MoS_2 data on Raman peak analysis is assembled in Table 1. All values are compared for the Raman analysis spots outside and inside of the wear tracks, as indicated in Table 1, to evaluate changes in thickness and crystallization of TMD due to the wear process. An increase in E_{2g} and A_{1g} peak spacing (from 25 cm^{-1} to 26.5 cm^{-1}) was observed when moving the Raman analysis spot from outside to inside the wear track only for tests conducted in ethanol. This increase can be attributed to a reduction in 2H MoS_2 layer thickness inside the wear track [32], which in the case of ethanol can be due to wear and removal of material to a very small thickness of less than 7–9 monolayers based on the peak spacing [32]. Both the dry nitrogen and dodecane wear tracks revealed no difference in peak spacing. However, a reduction of TMD thickness in the wear track may still have occurred. Peak spacing changes are only seen when transitioning from single to 7–9 mono-layer thick 2H MoS_2 with reductions in peak spacing reported in the range of 1–2 cm^{-1} [32]. The initial thickness of as-deposited 10–15 μm coatings would need to be reduced significantly to reach the few mono-layer thickness values sensitive to the E_{2g} and A_{1g} peak space analysis.

As can be seen from Table 1, both FWHM and peak intensity ratios increased when moving from outside to inside the wear track for tests conducted in the nitrogen and dodecane environments. Increases in FWHM can be attributed to grain refinement inside the wear track, whereas conversely, the test in the ethanol environment showed peak narrowing inside the wear track which corresponds with an increase in average grain size. Examinations of peak intensity ratios of the E_{2g} and A_{1g} in pristine molybdenite crystal showed an increase from approximately 0.4 to 0.7 when scanning the edge vs basal-plane oriented directions [29]. These ratios can potentially be used as a measure of crystalline orientation along the basal plane of worn MoS_2 surfaces. Both nitrogen and dodecane tests show an increase in E_{2g}/A_{1g} by a factor of 0.1, and both are within the 0.4–0.7 range, therefore a plausible explanation would be that randomly oriented microcrystalline powders are then reoriented such that basal planes are along the sliding direction, contributing to the low steady-state friction coefficients seen in Figs. 3 and 4 for these test environments. The test in ethanol has the opposite trend, with a decreasing E_{2g}/A_{1g} from 0.8 to 0.5. Notably, outside the wear track, the peak ratio is outside the given range for pristine molybdenite crystal, possibly indicating the peak ratios for polycrystalline and imperfect MoS_2, the signature for which may deviate from that of a pristine single crystal. It is possible that oxide formation could cause peak ratios to deviate from typical values.

There were no dominant oxide peaks present in Raman spectra outside or inside wear tracks for all test conditions (Fig. 7). A few weakly developed bands were present at 285 and 820 cm^{-1} for MoS_2 coatings and at 294 and 808 cm^{-1} for WS_2 coatings, which correspond to MoO_3 and WO_3 respectively. Their weak intensity and broad nature also indicate a poor degree of oxide phase crystallization. Interestingly, there was a reduction in the emergence of these oxide bands at the center of the wear tracks. This indicated that the initially oxidized components of the sprayed coating powder did not remain in the wear track and were removed from the sliding interface in the process of wear. Raman analysis has a limited sensitivity in analyzing oxides with low-crystalline order which could evolve in the wear track during the tests. An insight into the TMD coating oxidation was obtained from the results of the XPS analysis.

3.5. Chemical bonding evolution of wear track surfaces investigated with XPS analyses

To uncover the mechanism of the different behavior of the TMD in ethanol and dodecane environments, XPS analysis of the wear tracks on MoS_2 coatings was performed as a representative case. Samples of MoS_2 coatings were tested in both ethanol and dodecane for 5 m and 10 m of sliding distances respectively, and immediately thereafter, transferred for analysis in XPS. These shorter test durations were selected for wear track XPS analysis to ensure that the coatings were within steady-state COF regimes (see Fig. 4) and not worn through to expose the substrate, since in the case of ethanol this can happen already after 40 m sliding based on the COF recordings (Fig. 4, c). XPS results are presented in Fig. 8 for Mo 3d binding region scans and spectra for O 1s and S 2p region are presented in supplemental material as the discussion supporting information. The comparison provides insights into the oxidation wear and failure mechanisms of MoS_2 in ethanol and dodecane, where differences in peak constituent evolutions from 5 to 10 m of sliding can be most clearly seen in the Mo 3d spectra between ethanol and dodecane tests.

For the region with Mo $3d_{5/2}$ and Mo $3d_{3/2}$ doublets (Fig. 8), peak deconvolution indicates the primary presence of the Mo^{4+} oxidation state after 5 m of sliding. In the case of sliding tests in ethanol, an increase in the Mo^{6+} oxidation state was clearly observed after a 10 m sliding distance. This increased Mo^{6+} oxidation state suggests a rapid transition of MoS_2 to MoO_3 at the contact interface. It is then clear that in ethanol, a rapid oxidation of MoS_2 coating occurred inside the wear tracks leading to the formation of MoO_3, which resulted in a high coefficient of friction and an acceleration in the removal of the coating. In contrast, the TMD lubricant was prevented from oxidation in dodecane, leading to a similar low friction behavior to the one measured in dry nitrogen environments. There are two potential sources of oxidation of lubricant in ethanol as compared to dodecane: firstly, from the ethanol molecule, which can directly react with MoS_2 to form MoO_3. MoO_3 can

Table 1
E_{2g} (in plane) and A_{1g} (out of plane) Raman peak information for analyses performed inside and outside of wear tracks on MoS_2 coating surface after tests in dry nitrogen (control test), ethanol, and dodecane environments.

MoS_2 Environment	Difference in E_{2g} and A_{1g} center lines, outside wear track (cm^{-1})	Difference in E_{2g} and A_{1g} center lines, inside wear track (cm^{-1})	Difference in E_{2g} FWHM for outside vs. inside wear track (cm^{-1})	Difference in A_{1g} FWHM for outside vs. inside wear track (cm^{-1})	E_{2g}/A_{1g} intensity ratio, outside wear track	E_{2g}/A_{1g} intensity ratio, inside wear track
Dry Nitrogen	25.5	25.5	-1.5	-1.5	0.46	0.55
Ethanol	25	26.5	2	5	0.8	0.5
Dodecane	26	26	-2.5	-2	0.65	0.75

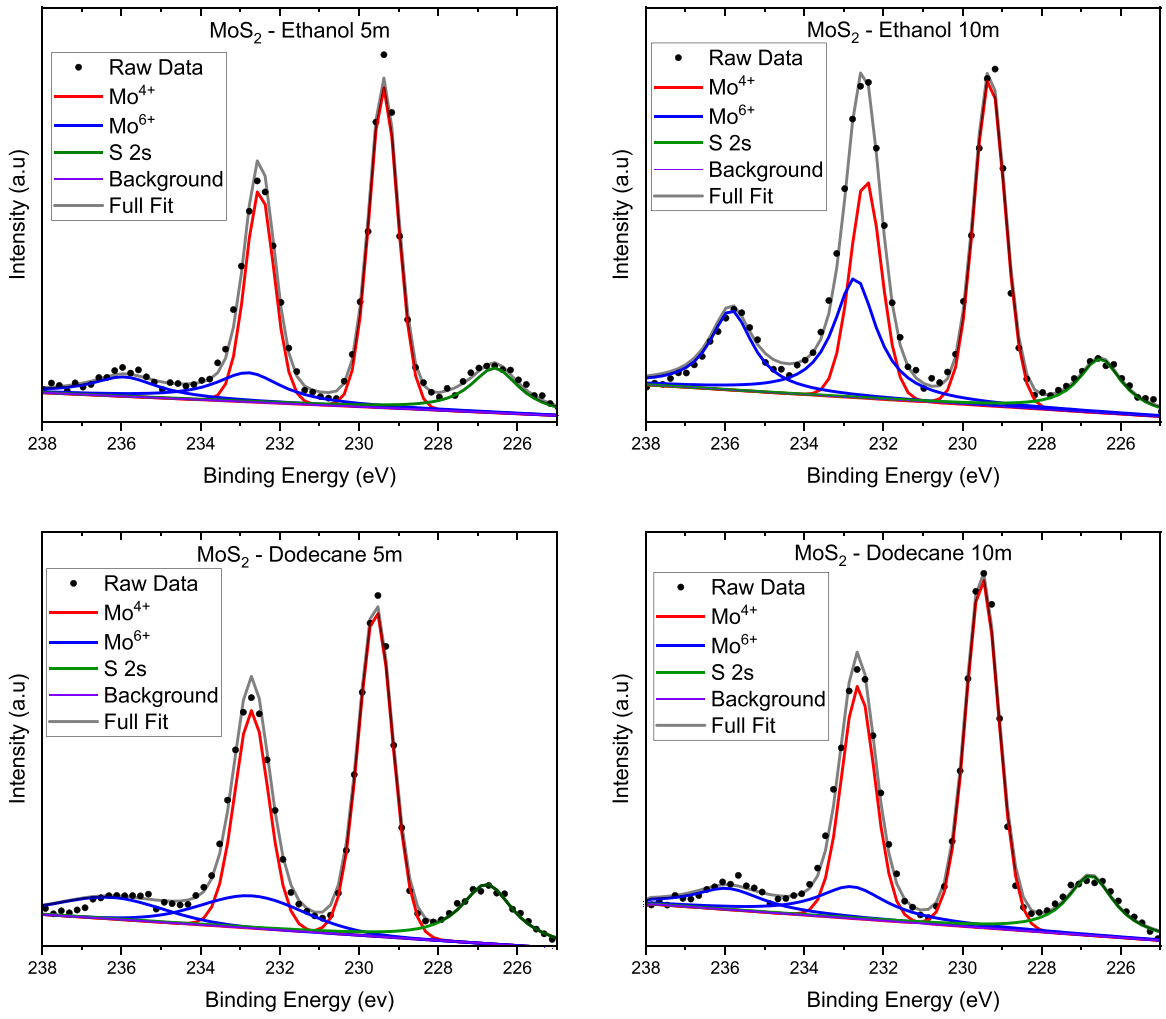

Fig. 8. XPS spectra in Mo 3d region obtained from inside wear tracks of MoS_2 coatings after 5 m and 10 m sliding in ethanol (top two) and dodecane (bottom two) with spectra fitting components indicated in the data legend.

then detach from the loosely bonded powder coating structure and form wear debris. Secondly, dodecane is hydrophobic and ethanol is hydrophilic. Thus, for ethanol sliding tests, both water and oxygen can diffuse through the ethanol bath and affect the TMD in the sliding contact surface, causing oxidation and disruption of the easy basal-plane shearing lubrication mechanism preventing the benefit of TMD-based lubrication as established for this class solid lubricant materials [21].

4. Conclusions

In this study, the tribological performance of MoS_2 and WS_2 coatings were compared in humid air, dry nitrogen, and immersion in ethanol and dodecane environments. The tests conducted in dry nitrogen and humid air revealed the expected behavior of TMDs, with a transfer film formation and low friction in dry nitrogen conditions, and a higher evolving friction in humid air conditions due to the ongoing oxidation. Using these control test environments, the impact of ethanol and dodecane on the tribological performance of TMDs was differentiated. The analysis of friction variation over the sliding distance, supported by optical imaging, EDS, and Raman of the wear tracks showed the rapid removal of both TMD coatings in the ethanol environment which led to high friction matching that of steel-on-steel sliding, as compared to the dodecane environment which maintained low friction throughout the tests. XPS analyses provided a clear evidence that the oxidation inside the wear track was significantly enhanced in the case of ethanol tests, corresponding to the increased oxidative wear and higher friction. In the case of dodecane tests, the coating showed much less evidence of oxidation, which was linked to the hydrophobic nature of dodecane, allowing for the formation and retention of the TMD transfer film in the contact, yielding tribological behavior like that of the dry nitrogen condition. Following the analogy with the well-established and similar behavior of TMDs in dry nitrogen, it is proposed that in dodecane, basal planes sheared easily due to the absence of water vapor and allowed for the orientation of basal planes parallel to the sliding direction. This reorientation of basal planes resulted in coefficients of friction significantly less than 0.1 with stable low friction maintained throughout the test. This study demonstrates that TMD coatings have a potential to be used as a protective coating in low viscosity hydrocarbon environments, but attention needs to be given to the chemical-molecular nature of the fuel to maximize the TMD potential in lubrication and survivability.

Statement of originality

As corresponding author, I, Andrey Voevodin, hereby confirm on behalf of all authors that: 1) The paper has not been published previously, that it is not under consideration for publication elsewhere, and that if accepted it will not be published elsewhere in the same form, in English or in any other language, without the written consent of the publisher. 2) The paper does not contain material which has been published previously, by the current authors or by others, of which the source is not explicitly cited in the paper.

Declaration of Competing Interest

The authors declare that they have no known competing financial interests or personal relationships that could have appeared to influence the work reported in this paper.

Data Availability

Data will be made available on request.

Acknowledgments

Research was sponsored by the Army Research Laboratory and was accomplished under Cooperative Agreement Number W911NF-20-2-0198 and W911NF-20-2-0249. The views and conclusions contained in this document are those of the authors and should not be interpreted as representing the official policies, either expressed or implied, of the Army Research Laboratory or the U.S. Government. The U.S. Government is authorized to reproduce and distribute reprints for Government purposes notwithstanding any copyright notation herein. This work was performed in part at the University of North Texas' Materials Research Facility. We thank Maddox Dockins, James Rodriquez, Austin Killiam, and Vanessa Montoya, and Nikhil Murthy for their assistance in completing this work.

Appendix A. Supporting information

Supplementary data associated with this article can be found in the online version at doi:10.1016/j.triboint.2022.108206.

References

[1] Donnet C, Erdemir A. Historical developments and new trends in tribological and solid lubricant coatings. Surf Coat Technol 2004;180–181:76–84. https://doi.org/10.1016/j.surfcoat.2003.10.022.
[2] Zhu S, Cheng J, Qiao Z, Yang J. High temperature solid-lubricating materials: a review. Tribol Int 2019;133:206–23. https://doi.org/10.1016/j.triboint.2018.12.037.
[3] Spalvins T. A review of recent advances in solid film lubrication. J. Vacuum Sci. Technol. A 1987. https://doi.org/10.1116/1.574106.
[4] Layered 2D Nanomaterials to Tailor Friction and Wear in Machine Elements—A Review - Marian - 2022 - Advanced Materials Interfaces - Wiley Online Library n.d. https://onlinelibrary.wiley.com/doi/epdf/10.1002/admi.202101622 (Accessed June 14 June 2022).
[5] McGuire N. Solid coatings: Not just for space vehicles anymore. Tribol Lubr Technol 2020;76(38–40):42–4. 46,48.
[6] Midson S , Korenyi-Both A , Clarke K Lubricious Thin-Film Coatings for Forging Applications: A Literature Review n.d.:40.
[7] Voevodin AA, Zabinski JS. Nanocomposite and nanostructured tribological materials for space applications. Compos Sci Technol 2005;65:741–8. https://doi.org/10.1016/j.compscitech.2004.10.008.
[8] Voevodin AA, O'Neill JP, Zabinski JS. Nanocomposite tribological coatings for aerospace applications. Surf Coat Technol 1999;116–119:36–45. https://doi.org/10.1016/S0257-8972(99)00228-5.
[9] Erdemir A. Review of engineered tribological interfaces for improved boundary lubrication. Tribol Int 2005;vol. 38:249–56. https://doi.org/10.1016/j.triboint.2004.08.008.
[10] Berman D, Erdemir A, Sumant AV. Approaches for achieving superlubricity in two-dimensional materials. ACS Nano 2018;12:2122–37. https://doi.org/10.1021/acsnano.7b09046.
[11] Scharf TW, Prasad SV. Solid lubricants: a review. J Mater Sci 2013;48:511–31. https://doi.org/10.1007/s10853-012-7038-2.
[12] Khare HS, Burris DL. Surface and subsurface contributions of oxidation and moisture to room temperature friction of molybdenum disulfide. Tribol Lett 2014;53:329–36. https://doi.org/10.1007/s11249-013-0273-0.
[13] Spalvins Z. Lubrication with sputtered MoS2 films. Princ,Oper, Limit 1992;vol. 1.
[14] Vazirisereshk MR, Martini A, Strubbe DA, Baykara MZ. Solid lubrication with MOS2: a review. ArXiv 2019.
[15] Watanabe S, Noshiro J, Miyake S. Tribological characteristics of WS2/MoS2 solid lubricating multilayer films. Surf Coat Technol 2004;183:347–51. https://doi.org/10.1016/j.surfcoat.2003.09.063.
[16] Christopher Muratore Andrey AVoevodin. Chameleon coatings: adaptive surfaces to reduce friction and wear in extreme environments. Annu Rev Mater Res 2009;39:297–324. https://doi.org/10.1146/annurev-matsci-082908-145259.
[17] Shirani A, Joy T, Rogov A, Lin M, Yerokhin A, Mogonye JE, et al. PEO-Chameleon as a potential protective coating on cast aluminum alloys for high-temperature applications. Surf Coat Technol 2020;397:126016. https://doi.org/10.1016/j.surfcoat.2020.126016.
[18] Claerbout VEP, Nicolini P, Polcar T. Exploring nanoscale lubrication mechanisms of multilayer MoS2 during sliding: the effect of humidity. Front Chem 2021;9. https://doi.org/10.3389/fchem.2021.684441.
[19] Curry J F Friction and Environmental Sensitivity of Molybdenum Disulfide: Effects of Microstructure. Lehigh, n.d.
[20] Siming Ren Kedong Shang, Mingjun Cui Liping Wang, Jibin Pu Peiyun Yi, et al. Structural design of MoS 2 -based coatings toward high humidity and wide temperature. J Mater Sci 2019;54:11889–902. https://doi.org/10.1007/s10853-019-03754-8.
[21] Claerbout Victor EP, Nicolini Paolo, Polcar Tomas. Exploring nanoscale lubrication mechanisms of multilayer MoS2 during sliding: the effect of humidity. Front Chem 2021;9. https://doi.org/10.3389/fchem.2021.684441.
[22] Kubart Tomas, Polcar Tomas, Kopecký L, Novak Rudolf, Nováková D. Temperature dependence of tribological properties of MoS2 and MoSe2 coatings. Surf Coat Technol 2005;193:230–3. https://doi.org/10.1016/j.surfcoat.2004.08.146.
[23] Sgroi MF, Asti M, Gili F, Deorsola FA, Bensaid S, Fino D, et al. Engine bench and road testing of an engine oil containing MoS2 particles as nano-additive for friction reduction. Tribol Int 2017;105:317–25. https://doi.org/10.1016/j.triboint.2016.10.013.
[24] Singh H, Mutyala KC, Doll GL. Rolling contact performance of a Ti-Containing MoS2 coating operating under ambient, vacuum, and oil-lubricated conditions. Coatings 2019;9:752. https://doi.org/10.3390/coatings9110752.
[25] Jacques K, Murthy N, Dixit S, Berman D, Berkebile S. Method for tribological experiment to study scuffing initiation on AISI 52100 steel and hard ceramic coatings. Tribol Int 2021;160:107001. https://doi.org/10.1016/j.triboint.2021.107001.
[26] Zhao X, Zhang G, Wang L, Xue Q. The tribological mechanism of MoS2 film under different humidity. Tribol Lett 2017:65. https://doi.org/10.1007/S11249-017-0847-3.
[27] Kohlhauser B, Ripoll MR, Riedl H, Koller CM, Koutna N, Amsüss A, et al. How to get noWear ? – A new take on the design of in-situ formed high performing low-friction tribo fi lms. Mater Des 2020;190:108519. https://doi.org/10.1016/j.matdes.2020.108519.
[28] Curry JF, Argibay N, Babuska T, Nation B, Martini A, Strandwitz NC, et al. Highly oriented MoS2 coatings: tribology and environmental stability. Tribol Lett 2016;64:1–9. https://doi.org/10.1007/s11249-016-0745-0.
[29] Tan SM, Ambrosi A, Sofer Z, Huber Š, Sedmidubský D, Pumera M. Pristine basal- and edge-plane-oriented molybdenite MoS2 exhibiting highly anisotropic properties. Chem – Eur J 2015;21:7170–8. https://doi.org/10.1002/chem.201500435.
[30] Windom BC, Sawyer WG, Hahn DW. A raman spectroscopic study of MoS 2 and MoO 3: applications to tribological systems. Tribol Lett 2011;42:301–10. https://doi.org/10.1007/s11249-011-9774-x.
[31] McDevitt NT, Zabinski JS, Donley MS, Bultman JE. Disorder-induced low-frequency Raman band observed in deposited MoS 2 films. Appl Spectrosc 1994;48:733–6. https://doi.org/10.1366/000370294774369063.
[32] Lee C, Yan H, Brus LE, Heinz TF, Hone J, Ryu S. Anomalous lattice vibrations of single- and few-layer MoS $_2$. ACS Nano 2010;4:2695–700. https://doi.org/10.1021/nn1003937.